

# Dark, heat-reflective, anti-ice rain and superhydrophobic cement concrete surfaces

Zhu Chenxi, Lv Jian, Chen Lingdong, Lin Weiqiang, Zhang Jing, Yang Jintao<sup>\*</sup>, Feng Jie<sup>\*</sup>

College of Materials Science and Engineering, Zhejiang University of Technology, Hangzhou, China

## HIGHLIGHTS

- Heat-reflective and superhydrophobic cement concrete surface were prepared.
- The surface has high infrared reflectance approaching that of the white TiO<sub>2</sub>.
- The superhydrophobic properties exhibit good stability to rain and UV exposure.
- The superhydrophobic surface has good anti-ice rain properties under −12 °C.
- The surface has great potential in the exterior of building walls or roofs.

## ARTICLE INFO

### Article history:

Received 30 August 2018  
Received in revised form 27 May 2019  
Accepted 30 May 2019  
Available online 5 June 2019

### Keywords:

Cement concrete  
Heat-reflective  
Superhydrophobic  
Anti-ice rain

## ABSTRACT

Antifouling, weatherable, and heat-reflective coatings have much value for solar sheltering of building in summer. In this work, a multifunctional cement mortar mixture was obtained by mixing “cool cold” black pigments with cement, sand, TiO<sub>2</sub> nanoparticles and water. After the mixture was mortared on a cement concrete slab, dried at room temperature and treated with fluorine silicon sol, a gray cement concrete layer was obtained. UV–visible–infrared spectrometer confirmed that the layer has obvious infrared-reflective property at 780–2500 nm. Under the radiation of a 275 W and 40 cm height infrared lamp, the surface temperature of the gray “cool cold” cement concrete is about 40 °C lower than that of the carbon black cement concrete, and is about 20 °C lower than that of the ordinary cement concrete, and is only about 1 °C higher than that of the white TiO<sub>2</sub> cement concrete. Moreover, all these cement concrete surfaces showed typical superhydrophobic (SH) property and the “cool cold” cement concrete surface further exhibited stable SH properties to both rain and UV radiation, which may allow for self-cleaning performance for the surface and the ability to retain its heat-reflective property over a long period of time. Meanwhile, the “cool cold” cement concrete SH surface exhibited excellent anti-ice rain performance. Because the layer can be easily mortared on the cement concrete substrate, we think it would have great potential for use on building roof and outside walls to reduce air-conditioning energy consumption in the summer.

© 2019 Elsevier Ltd. All rights reserved.

## 1. Introduction

Due to the rapid increase of building energy consumption, which accounts for nearly approximately one-third of total societal energy consumption [1], it is important to seek some effective methods to realize building energy saving [2,3]. Recently, enhancing the infrared reflectance of the exterior wall or roof has been studied and adopted to solve this problem, because the infrared energy accounts for approximately half of the total solar energy [4]. So far, white or light color coatings [5,6] have been widely

applied on the exterior of building walls or roofs because it is well known that white color possesses the best solar reflective performance [7].

However, the white or light color always has the problem of being easily polluted and single color, hardly satisfies human demand in actual building decoration. In recent years, more and more deep color pigments which possess excellent infrared reflective property have been developed, such as blue [8], yellow [9], red [10] and so on. To apply these infrared reflective pigments in the field of building exterior wall or roof, some researchers introduced these pigments into organic coating and prepared infrared reflective coatings [11,12]. And the inorganic infrared reflective coatings such as cement concrete have also been prepared [13,14].

<sup>\*</sup> Corresponding authors.

E-mail addresses: [yangjt@zjut.edu.cn](mailto:yangjt@zjut.edu.cn) (J. Yang), [fengjie@zjut.edu.cn](mailto:fengjie@zjut.edu.cn) (J. Feng).

Coating surfaces exposed in the actual outdoor environment will be polluted by dust deposition, which generally reduces the infrared reflectance [15]. As a result, much manpower and energy may be consumed to clean the polluted surface [16]. It is well known that superhydrophobic (SH) surfaces possess the self-cleaning ability due to micro roughness and low surface energy [17–19]. Some deep color, SH and infrared reflective organic coatings have been prepared recently [20–22] and they all show excellent self-clean property. However, organic coatings have poor UV resistance when they are used on building exterior wall or roof. Different with common coatings, SH coating is sensitive to UV aging because once micro- or nano-cracks appear on the coating surface caused by UV aging, water droplets would adhere on the surface.

Based on mature methods of SH surface preparation, inorganic concrete SH surfaces have also been prepared in the past 5 years [23–28]. For example, Nosonovsky et al. synthesized SH concrete for the first time by applying hydrophobic emulsions on Portland cement mortar tiles [23]. Arabzadeh et al. created a skid-resistant SH coating on pavement by spraying different nanomaterials with different durations [25]. Gao et al. prepared SH and luminescent cement pavement materials by mixing the luminescent materials and hydrophobic materials with cement [26]. She et al. fabricated SH concrete surface by direct spraying nano-silica gel functionalized by low surface-energy surfactants to simultaneously modify the inherent multi-scale microstructure and surface chemical properties [28]. However, all these concrete SH surfaces have no infrared-reflective function.

Another advantage of SH surface is anti-icing and anti-ice rain property through reducing water droplets adhesion and heat exchange on it [29–36]. Eshaghi et al. confirmed that anti-icing property of SH glass was better than that of the general glass under  $-12\text{ }^{\circ}\text{C}$  [34]. In previous studies, our research group prepared the SH copper foils and elucidated the mechanism of jumping condensation and delayed frost growth on them [35]. Zhao et al. prepared the concrete SH surface through template method and demonstrated its anti-icing property under  $-5\text{ }^{\circ}\text{C}$  [36].

It is unavoidable for organic materials to be degraded and aged by ultraviolet (UV) light, oxygen and rain water [37,38]. As for organic SH coatings, degradation and weathering generally influence the SH property durability. Therefore, in this work, we prepared the heat-reflective and SH concrete inorganic layers just through simply adding  $\text{TiO}_2$  nanoparticles and black “cool cold” infrared reflective pigments into cement mortar, and followed by mortaring on a cement slab, drying at room temperature and finally treating with fluorine silicon sol. We convince that these inorganic coatings have great potential applications on building exterior wall and roof to reduce the energy consumption, especially in summer.

## 2. Experimental section

### 2.1. Materials

Portland cement (PO42.5R) was purchased from Guangdong Runhe Jiancai Co., Ltd. (China). Sand (70–90 mesh number,  $\sim 200\text{ }\mu\text{m}$  diameter) was purchased from Lingshou Hongfeng Co., Ltd. (China). Infrared reflective pigment (“cool cold” pigment-Black 30C941, which consist mostly of  $\text{CrO}_3$  and  $\text{Fe}_2\text{O}_3$ ) with diameter  $\sim 0.5\text{ }\mu\text{m}$  was obtained from Shepherd Color Company (USA). Nano  $\text{TiO}_2$  (R-105) was purchased from Dupont Company (USA). Carbon black (N234) was supplied by Zhongce Rubber Co., Ltd. (China). 1H, 1H, 2H, 2H-Perfluorodecyltriethoxysilane (FAS) was purchased from Sicong New Material Ltd (Quanzhou, China). All

other chemicals were general sale products and were used directly after being received.

### 2.2. Preparation of the cement concrete layers

A certain amount of Portland cement, sand, Nano  $\text{TiO}_2$ , black “cool cold” pigment or carbon black (CB) was added into a beaker according to the specific formulation (Table 1) and mixed by hand with a small trowel for 10 min till the color became uniformly. Then 5.2 g water was added and the mixture was stirred by the trowel to get cement mortar. The cement mortar was daubed on a  $10\text{ cm} \times 10\text{ cm}$  cement slab with a trowel and cured at room temperature for 36 h. After that, 1 mL of FAS was added into 70 mL water/ethanol mixed solution (40 mL water and 30 mL ethanol) with stirring and 1 mol/L dilute hydrochloric acid were used to adjust the pH value of the solution to about 4. After stirring for another 2 h at room temperature, the FAS sol was created. The dried cement concrete layers were wetted with the FAS sol and dried at  $120\text{ }^{\circ}\text{C}$  for 1 h to get SH cement concrete layers (Fig. 1).

### 2.3. Characterization

The infrared-reflective properties of the cement concrete layers were measured by UV–visible–infrared spectrometer (Lambda750, PE Company, USA). To simulate heat-reflective property, the layers were placed on a polystyrene (PS) foam board under a 275-W infrared lamp (Fig. 2) or under solar radiation, and changes in surface temperature were recorded. Here the PS foam was used to avoid the heat of the layers transferring to the substrates. The sample was irradiated by the infrared lamp for 20 min and the surface temperature per minute was measured though an infrared thermometer. Then the lamp was turn off and the temperature was continuously followed for another 10 min.

The surface morphology of the layers was characterized via field emission scanning electron microscopy (F-SEM, NovaNano450, FEI). The wettability of the layers was tested by measuring the water contact angle (WCA) and sliding angle (SA) using the contact-angle system (OCA35, German Dataphysics) with  $4\text{ }\mu\text{L}$  deionized water droplets. Each layer was measured five times and the average values were obtained.

The stability of the SH property towards UV radiation was measured by placing the SH layer under a 36-W UV lamp (340 nm wavelength, radiation strength at  $1.0\text{ W}/\text{cm}^2$ ) for 3 months and recording wettability to flowing water every 1–15 days. The stability of the SH property to water impact was observed in the middle of the rain ( $16.5\text{ mm}/24\text{ h}$ ). The layer was placed at  $30^{\circ}$  obliquity and rain drops impacting and adhering to the layer surface were recorded with video. For more accurate evaluation, The WCAs and SAs of the layer surface after raining for different time were measured.

The layers' anti-ice rain test device is shown in Fig. 3. By controlling temperatures of the Peltier Thermoelectric Cooler stage at  $-5\text{ }^{\circ}\text{C}$  to  $-25\text{ }^{\circ}\text{C}$ , the surface temperatures of the cement concrete layers were controlled from  $-2$  to  $-17\text{ }^{\circ}\text{C}$ . Through a syringe and a long and fine pinhead, ice-water mixture was dropped onto the layer surfaces. The drop diameter was 3–5 mm and the drop-

**Table 1**  
The typical formulation of cement concrete layers (g).

Samples	Cement	Sand	Nano $\text{TiO}_2$	Black “cool cold” pigment	CB
1	10	15	2	2	0
2	10	15	2	4	0
3	10	15	2	6	0
4	10	15	4	0	0
5	10	15	0	0	4
6	10	15	0	0	0

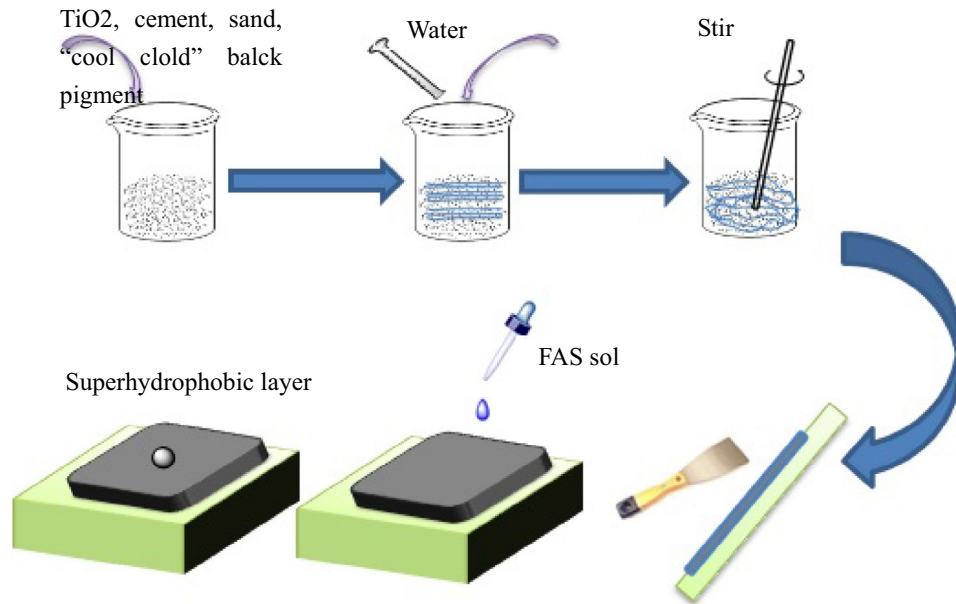


Fig. 1. Preparation process of the heat-reflective and SH cement concrete layer.

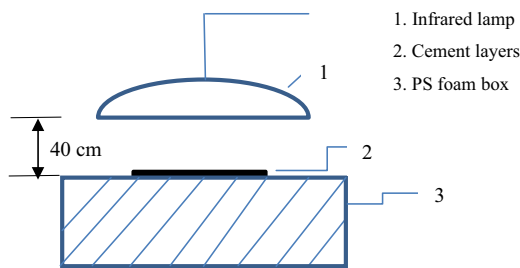


Fig. 2. Homemade device for measuring the infrared-reflective properties of the layers.

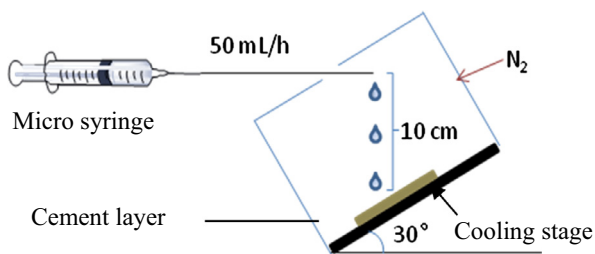


Fig. 3. Homemade device for measuring the anti-icing properties of the concrete SH layers.

ping rate was set to 50 mL/h. The whole system was semi-closed in a glass box with enough nitrogen atmosphere for preventing frost formation on the layer surface.

### 3. Results and discussion

#### 3.1. Infrared reflective properties of the cement concrete layers

As we all known, the energy of solar radiation is mainly concentrated in the visible region and the near infrared region. We measured the reflectance of the layers within the wavelength range from 250 nm to 2500 nm. As shown in Fig. 4, due to the addition of black “cool cold” pigment, the “cool cold” cement concrete layers show high reflectance ( $\sim 40\%$ ) in the near infrared region

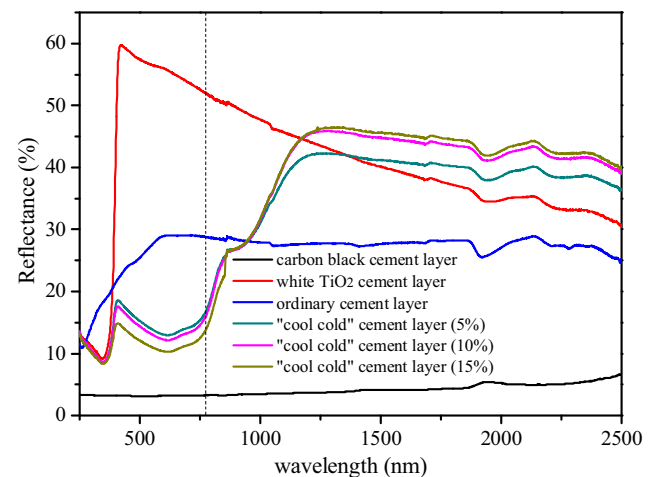


Fig. 4. The UV-visible-infrared reflectance of different cement layers.

(780 nm to 2500 nm) compared with the ordinary cement concrete layer ( $\sim 28\%$ ). Moreover, the higher “cool cold” pigment content, the higher the infrared reflectance. In the range between 1200 nm and 2500 nm, the reflectances of the black “cool cold” cement concrete layers are even higher than that of the white  $\text{TiO}_2$  cement concrete layer.

However, there is no significant difference between the infrared reflectances of the “cool cold” cement concrete layers containing 10 wt% and 15 wt% pigments. Therefore, with regards to its low cost, the “cool cold” layer (10 wt%) is the best formula and was used to carry out subsequent experiments. Although the white  $\text{TiO}_2$  cement concrete layer has higher reflectance in the whole wavelength range due to the contribution of visible light, the gray “cool cold” cement concrete layer is still necessary in many application situations for its deep color, otherwise carbon black cement concrete layer showed lowest reflectance (5 wt%).

To study the heat-reflective property of “cool cold” black cement concrete layers more intuitively, the surface temperatures of the layers under infrared lamp radiation were measured. As shown in Fig. 5, compared with the white  $\text{TiO}_2$  cement concrete

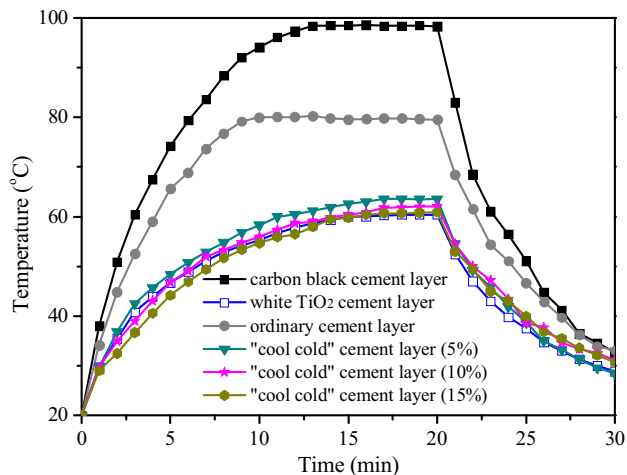


Fig. 5. Surface temperatures of the cement concrete layers vs infrared lamp radiation time.

layer, the “cool cold” layers exhibit the near surface temperatures. The surface temperature of the gray “cool cold” concrete layer containing 5 wt% “cool cold pigment” is about 40 °C lower than that of the carbon black concrete layer, and is about 20 °C lower than that of the ordinary concrete layer, and is only about 1 °C higher than that of the white TiO<sub>2</sub> concrete layer. These results are the same trend to the results shown in Fig. 4, implying excellent heat reflectance of “cool cold” concrete layers.

To investigate the real heat-reflective effect of the “cool cold” concrete layers in the actual environment, we measured the surface temperature of the layers under the solar radiation from 9:00 am to 3:00 pm with the highest air temperature of 25 °C (Fig. 6). Same as the results shown in Fig. 5, the white TiO<sub>2</sub> concrete layer shows the lowest surface temperature and the best heat-reflective effect. On the contrary, the carbon black concrete layer shows the worst heat-reflective effect. The surface temperature of the “cool cold” layer (10–15 wt%) is 8 °C and 17 °C lower than the ordinary concrete layer and the carbon black concrete layer, respectively. These two data are both smaller than those measured under infrared lamp (Fig. 5), where the corresponding difference are 20 °C and 40 °C, respectively. This is because visible light energy accounts for half of the whole solar energy and these three layers all adsorb most of visible light energy. Due to the same reason, the surface temperature of “cool cold” layer is about 3–5 °C higher than that of white TiO<sub>2</sub> concrete layer.

### 3.2. Morphology and wettability of the coatings

The surface morphologies of all cement concrete layers are shown in Figs. 7 and 8. As shown in Fig. 7, the surfaces of the TiO<sub>2</sub> layer and carbon black layer both show micro- and nano roughness structures due to aggregation of nanoparticles. There is no obvious nano structure on the ordinary concrete layer surface due to the lack of nanoparticles. However, due to the decoration of FAS, all the three layers surfaces exhibit typical SH property. The WCA and SA of the TiO<sub>2</sub> layer surface are  $151.8^\circ \pm 0.6^\circ$  and  $5.4^\circ \pm 1.2^\circ$ , respectively. The WCA and SA of the carbon black layer surface are  $153.2^\circ \pm 1.1^\circ$  and  $3.8^\circ \pm 1.0^\circ$ , respectively. And the WCA and SA of the ordinary concrete layer surface is also  $150.4^\circ \pm 0.3^\circ$  and  $8.9^\circ \pm 2.2^\circ$ , respectively.

Fig. 8 shows the surface morphologies of the “cool cold” cement concrete layers with different “cool cold” pigment content. On the “cool cold” layer surface, the nano TiO<sub>2</sub>, the “cool cold” pigments and the sands together form the micro- and nano roughness structures. Following an increase in “cool cold” pigment content, more submicron structures appear. Similar with other cement concrete layer surfaces, all the “cool cold” layer surfaces exhibit the typical SH properties, e.g., with CAs all bigger than 150° and SAs all smaller than 10°.

### 3.3. The stability of the SH property to rain and UV radiation

Due to being used on roof or exterior wall, it is unavoidable that the cement concrete layer will be scoured by rain in the actual environment. We placed the “cool cold” layer (10.0 wt%) in the rain to test its outdoor rain-resistance ability. Representative images taken during rainfall are shown in Fig. 9. The results showed that after 2 h rain, the whole surface was completely dry and there are no rain droplets adhering on the surface. Most of the raindrops bounced off the surface of the layer (see Supplementary data, Movie S1). After 6 h, there were a few rain droplets on the surface (in the red circle) at concave sites. However, these rain droplets could be taken away by the subsequent drops. This test shows that our concrete layer can keep stable SH property in the rain environment and endow exterior wall self-cleaning prospectively. We also measured the WCAs and SAs of the layer after being subjected to rain over different time periods. The results are shown in Fig. 10. The results further prove that the layer surface can keep SH property within 6 h raining. The possible reason is that unlike SH coating formed by organic resin especially from waterborne resin [18], there is no polar groups in the inorganic concrete layer surface thus its SH property is stable to raining.



Video S1.

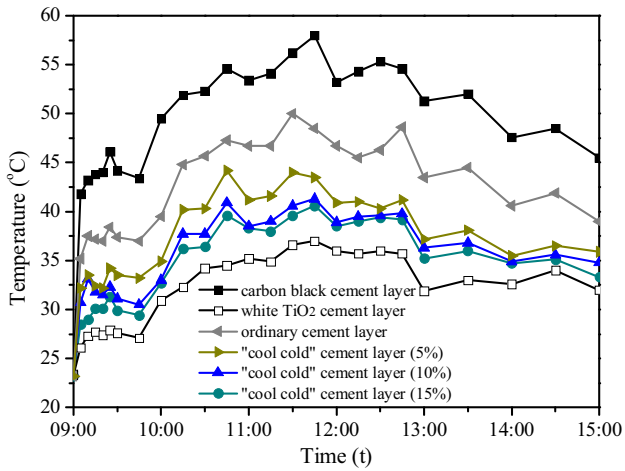


**Fig. 6.** Surface temperature changes of the cement concrete layers vs solar radiation time.

Another requirement for an SH coat is UV resistance. Compared with organic coating, concrete layer should be much more stable to UV exposure. In another study, we measured the UV resistance of concrete SH surface, which possesses the same formulation with the ordinary concrete layer studied here. The results showed that

after 68 days UV radiation or 40 days outdoor natural weathering, the surface still exhibited typical SH property (see [Supplementary data](#), [Movie S2](#) and [S3](#)).



**Video S2.**



**Video S3.**

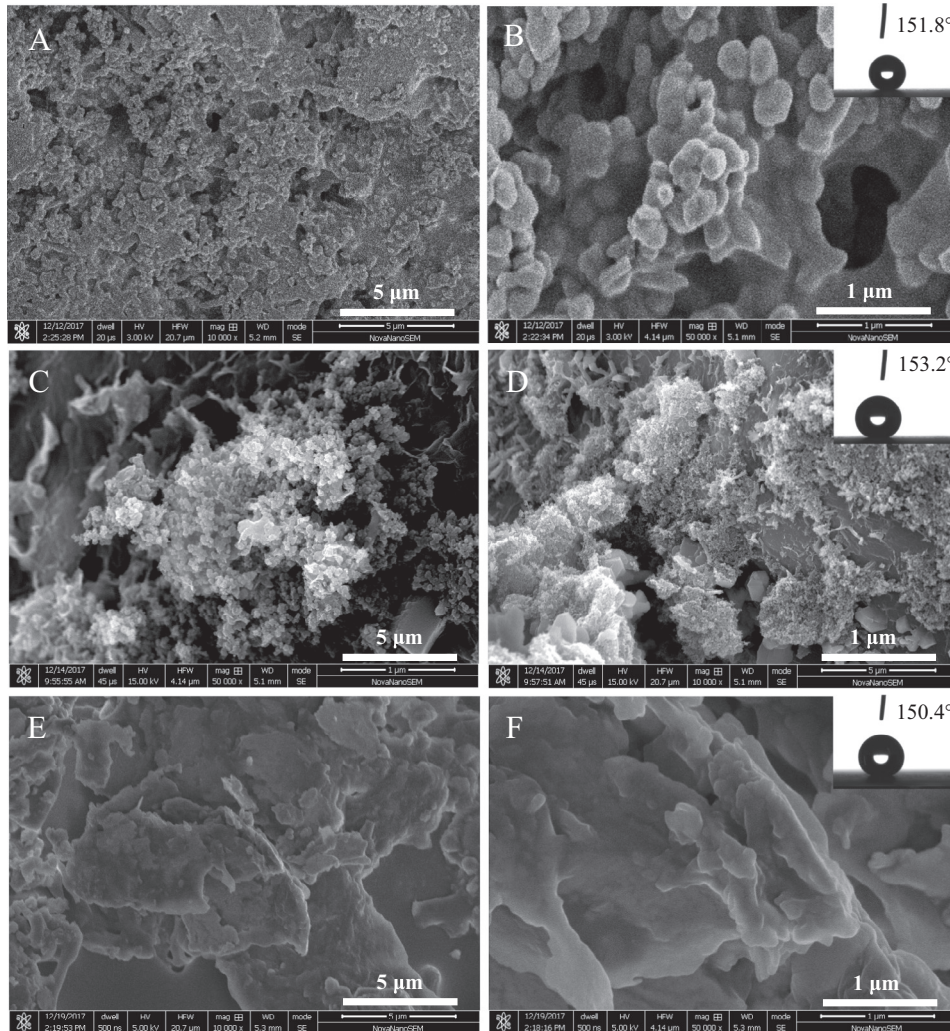


**Fig. 7.** Surface SEM images of white TiO<sub>2</sub> cement concrete layer (A/B), carbon black concrete layer (C/D), ordinary concrete layer (E/F). B, D, F are magnified images of A, C, E, respectively. The insets are profiles of 4 μL water drops on coatings, showing CAs all larger than 150°.

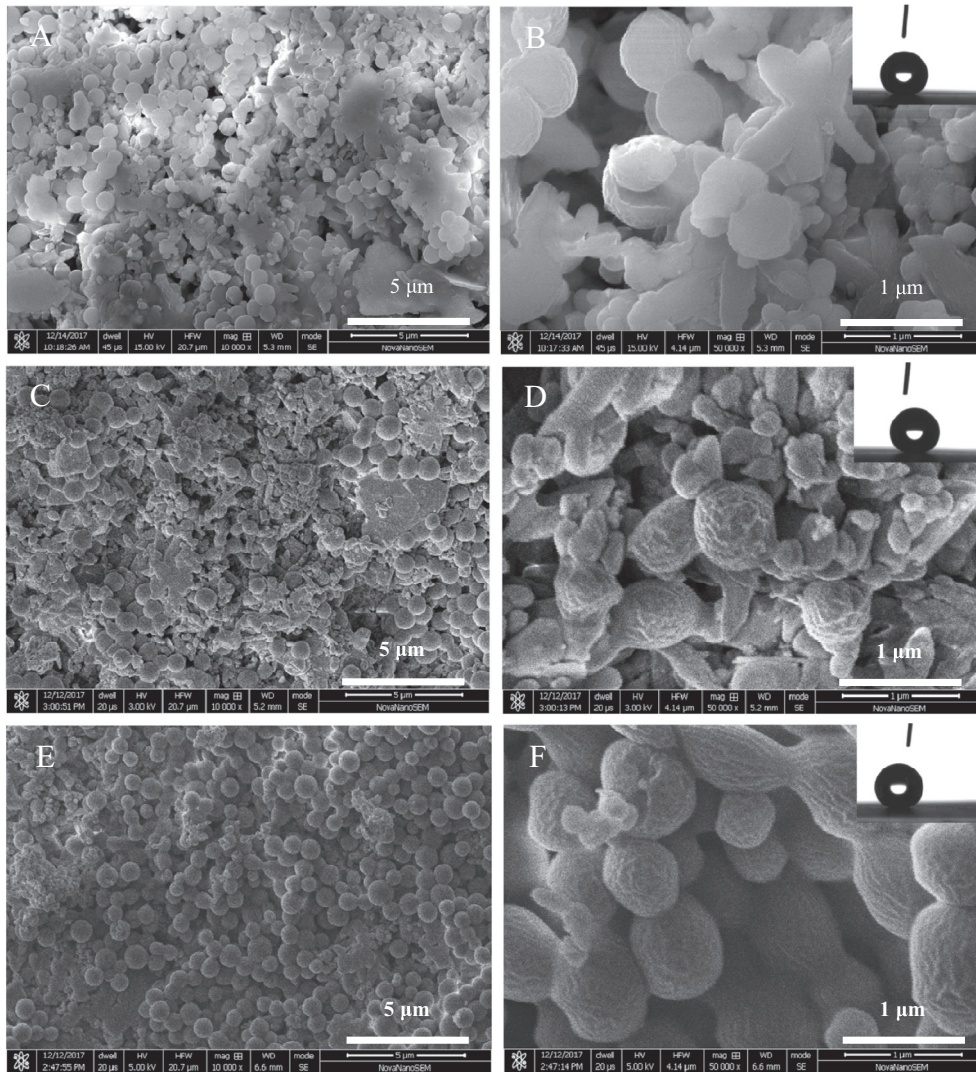


**Fig. 8.** SEM images of cement concrete layers with different “cool cold” pigment contents. A/B: 5 wt%; C/D: 10 wt%; E/F: 15 wt%. B, D, F are magnified images of A, C, E, respectively. The insets are profiles of 4  $\mu\text{L}$  water drops on coatings, showing CAs all larger than  $150^\circ$ .

### 3.4. Anti-ice rain property of the cement concrete layer

The anti-ice rain property of SH surfaces is always been desirable, especially for the cement concrete exterior wall [29–36]. We tested the anti-ice rain performance of “cool cold” cement concrete layer (10 wt%) surface using the device shown in Fig. 3. The results are displayed in Figs. 11 and 12. When the surface temperature of the layer is descended to  $-2^\circ\text{C}$ ,  $-7^\circ\text{C}$  or  $-12^\circ\text{C}$ , neither subcooled water droplets nor freezing beads or frosting are found on the surface in 1 h trial. After 1 h trial, the surface WCAs are all larger than  $150^\circ$  and the SAs all less than  $10^\circ$  (Fig. 11). This demonstrates that the layers can resist ice rain at least at  $-12^\circ\text{C}$ . In winter of cold region, such resistance can protect concrete surface against freeze-thaw damage, a damage caused by icing of water penetrating in the nano-holes of surface [36].

However, when the surface temperature of the cement concrete layer is descended to  $-17^\circ\text{C}$ , freezing phenomenon appears on the layer surface and the freezing region no longer possesses SH property after the ice was thawed. However, after the wetted layer surface was dried at  $120^\circ\text{C}$  for 15 min, the SH property of the surface

is restored again (Fig. 12). This demonstrates that even at  $-17^\circ\text{C}$ , little freeze-thaw damage occurs on the cement concrete layer SH surface. The possible reason is that even the thawed water penetrated in the micro-gaps of SH surface, e.g., forms Wenzel state, but has not penetrated in the nano-holes of the surface, or the surface nanostructure may be damaged already.

In addition to the mixing process for the cement mortar described in Section 2.2, we also tried another mixing process, e.g., the nano  $\text{TiO}_2$  were firstly dispersed into water by stirring, ultrasonically treated (600 w) for 10 min. Then the resulted suspension was filled into the mixture of other solid constituents and the mortar was stirred with a manual trowel till the color became uniformly. The subsequent procedures were same as those described in the experimental part. The UV-visible-infrared reflectances of “cool cold” cement layer (15.0 wt%) prepared by two different process was compared. The results showed that there was no significant difference in the reflectance (see supplementary data, Fig. S1). To demonstrate the homogeneity of the constituents on the “cool cold” cement layer, we mapped the surface elements by SEM and found that Fe, Cr and Ti were

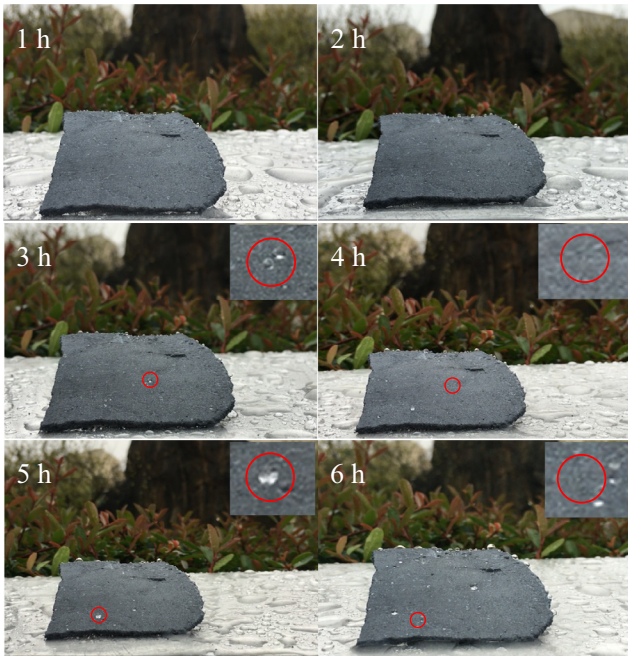


**Fig. 9.** Time-lapse optical images of the gray “cool cold” cement concrete layer surface during 6 h of rain (16.5 mm/24 h). Most of the impacting raindrops bounced off the surface, and a small amount adhered on the surface but can also be removed by subsequent drops (insets are magnification).

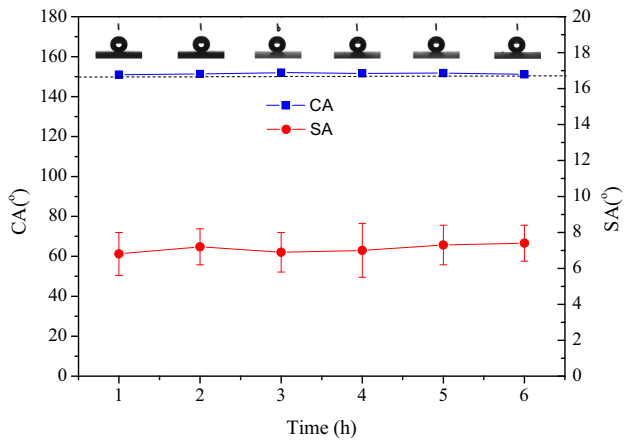


**Fig. 10.** The CAs and SAs of “cool cold” cement concrete layer surface (10.0 wt%) after being subjected to middle rain with different time.

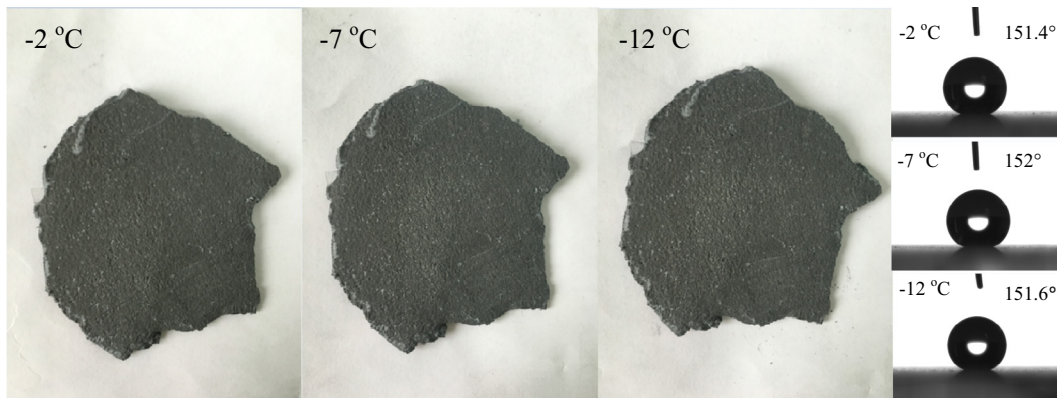


**Fig. 11.** Anti-ice rain performance of “cool cold” cement concrete layer surface (10 wt%) and CAs of the surface after 1 h anti-ice rain trial at different temperatures.

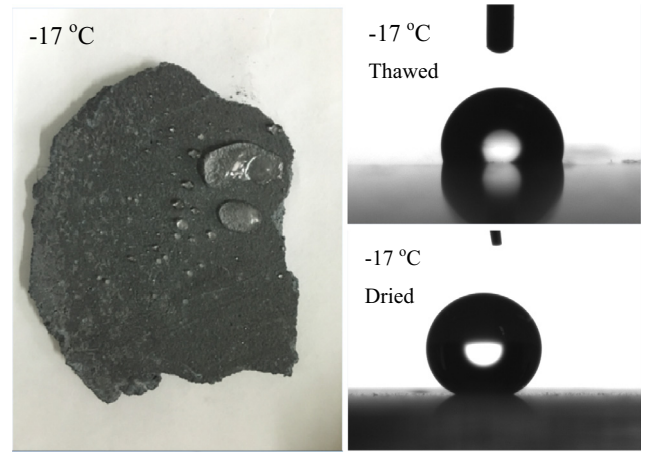


**Fig. 12.** Anti-ice rain property of the “cool cold” cement concrete layer (10 wt%) and the WCAs of area where the ice was thawed and the surface dried completely.

distributed homogeneously on both two types of layer surfaces (see [supplementary data, Figs. S2 and S3](#)). Fe and Cr are both from black “cool cold” pigment and Ti is from nano TiO<sub>2</sub>. This demonstrates that mixing by hands with suitable tool is feasible, which supplies great convenience for the worker in process of construction.

#### 4. Conclusions

We prepared heat-reflective and SH cement concrete surfaces through simply mixing nano TiO<sub>2</sub> and black “cool cold” infrared reflective pigments with cement mortar, and followed by drying and decorating with low surface energy FAS sol. These cement concrete surfaces possess high infrared reflectance approaching that of the white TiO<sub>2</sub> cement concrete surface and excellent heat-reflective properties either under infrared lamp or under solar radiation. Meanwhile, the cement concrete SH properties exhibit good stability to rain and UV exposure. Moreover, their anti-ice rain properties under −12 °C are also good. Although gray Portland cement was used here, white cement may also be adopted and should have better effect in reflecting infrared and solar energy. We believe that these multifunctional cement concrete surfaces would have great application potential in the field of exterior wall or roof for descending air-conditioning energy consumption.

## Declaration of Competing Interest

None.

## Acknowledgments

We gratefully acknowledge financial support from the National Natural Science Foundation of China (No. 51172206) and the Public Welfare Foundation from Zhejiang Province (2016C31011).

## Author contributions

Authors C.X. Zhu and J. Lv contributed equally.

## Appendix A. Supplementary data

Supplementary data to this article can be found online at <https://doi.org/10.1016/j.conbuildmat.2019.05.188>.

## References

- [1] G.A.E. Vandenbosch, Z.K. Ma, Upper bounds for the solar energy harvesting efficiency of nano-antennas, *Nano Energy* 1 (2012) 494–502.
- [2] H.X. Zhao, F. Magoulès, A review on the prediction of building energy consumption, *Renew. Sust. Energy Rev.* 16 (2012) 3586–3592.
- [3] A.I. Dounis, Artificial intelligence for energy conservation in buildings, *Adv. Build. Energy Res.* 4 (2010) 267–299.
- [4] R. Levinson, P. Berdahl, H. Akbari, Solar spectral optical properties of pigments—Part I: Model for deriving scattering and absorption coefficients from transmittance and reflectance measurements, *Sol. Energy Mater. Sol. Cells* 89 (2005) 319–349.
- [5] I. Roppolo, N. Shahzad, A. Sacco, E. Tresso, M. Sangermano, Multifunctional NIR-reflective and self-cleaning UV-cured coating for solar cell applications based on cycloaliphatic epoxy resin, *Prog. Org. Coat.* 77 (2014) 458–462.
- [6] Y.P. Wu, P. Krishnan, L.Y.E. Yu, M.H. Zhang, Using lightweight cement composite and photocatalytic coating to reduce cooling energy consumption of buildings, *Constr. Build. Mater.* 145 (2017) 555–564.
- [7] H. Akbari, M. Pomerantz, H. Taha, Cool surfaces and shade trees to reduce energy use and improve air quality in urban areas, *Sol. Energy* 70 (2001) 295–310.
- [8] R. Ianoş, E. Muntean, C. Păcurariu, R. Lazau, C. Bândas, G. Delinescu, Combustion synthesis of a blue co-doped zinc aluminate near-infrared reflective pigment, *Dyes Pigm.* 142 (2017) 24–31.
- [9] Y. Xiao, B. Huang, J.Q. Chen, X.Q. Sun, Novel Bi<sup>3+</sup>, doped and Bi<sup>3+</sup>/Tb<sup>3+</sup>, co-doped LaYO<sub>3</sub>, pigments with high near-infrared reflectances, *J. Alloys Compd.* 762 (2018) 873–880.
- [10] R. Yang, A.J. Han, M.Q. Ye, X.X. Chen, L. Yuan, Synthesis, characterization and thermal performance of Fe/N co-doped MgTiO<sub>3</sub> as a novel high near-infrared reflective pigment, *Sol. Energy Mater. Sol. Cells* 160 (2017) 307–318.
- [11] B. Huang, Y. Xiao, C. Huang, J.Q. Chen, X.Q. Sun, Environment-friendly pigments based on praseodymium and terbium doped La<sub>2</sub>Ce<sub>2</sub>O<sub>7</sub> with high near-infrared reflectance: synthesis and characterization, *Dyes Pigm.* 147 (2017) 225–233.
- [12] C. Ding, A.J. Han, M.Q. Ye, Y. Zhang, L.Y. Yao, J.L. Yang, Hydrothermal synthesis and characterization of novel yellow pigments based on V<sup>5+</sup> doped BiPO<sub>4</sub> with high near-infrared reflectance, *RSC Adv.* 8 (2018) 19690–19700.
- [13] F. Rosso, A.L. Pisello, V.L. Castaldo, C. Fabiani, F. Cotana, M. Ferrero, W. Jin, New cool concrete for building envelopes and urban paving: optics-energy and thermal assessment in dynamic conditions, *Energy Build.* 151 (2017) 381–392.
- [14] S. Sameera, P.P. Rao, S. Divya, A.K.V. Raj, T.R.A. Thara, High IR reflecting BiVO<sub>4</sub>-CaMoO<sub>4</sub> based yellow pigments for cool roof applications, *Energy Build.* 154 (2017) 491–498.
- [15] J. Zhang, C. Zhu, J. Lv, J. Feng, Preparation of colorful, infrared-reflective and superhydrophobic polymer films with obvious resistance to dust deposition, *ACS Appl. Mater. Interfaces* 10 (2018) 40219–40227.
- [16] Y.J. Lee, E.A. You, Y.G. Ha, Transparent, self-cleaning and waterproof surfaces with tunable micro/nano dual-scale structures, *Nanotechnology* 27 (2016) 355701–355708.
- [17] G. Wen, Z.G. Guo, W.M. Liu, Biomimetic polymeric superhydrophobic surfaces and nanostructures: from fabrication to applications, *Nanoscale* 9 (2017) 3338–3366.
- [18] J. Zhang, W.C. Zhang, J.J. Lu, C.X. Zhu, W.Q. Lin, J. Feng, Aqueous epoxy-based superhydrophobic coatings: fabrication and stability in water, *Prog. Organ. Coat.* 121 (2018) 201–208.
- [19] X.W. Kong, J. Zhang, Q. Xuan, J. Lu, J. Feng, Superhydrophobic coating for antifouling of Chinese paintings, *Langmuir* 34 (2018) 8294–8301.
- [20] J. Zhang, W.Q. Lin, C.X. Zhu, J. Lv, W.C. Zhang, J. Feng, Dark, infrared reflective and superhydrophobic coatings by waterborne resins, *Langmuir* 34 (2018) 5600–5605.
- [21] Z. Yang, X. Xue, J.G. Dai, Y.W. Li, J. Qin, Y. Feng, J. Qu, Z.Y. He, P.C. Sun, L.J. Xu, T. Zhang, T.J. Qu, W.D. Zhang, Study of a super-non-wetting self-cleaning solar reflective blue-grey paint coating with luminescence, *Sol. Energy Mater. Sol. Cells* 176 (2018) 69–80.
- [22] Q. Gao, X.M. Wu, Y.M. Fan, Q.L. Meng, Novel near infrared reflective pigments based on hollow glass microsphere/BiOCl<sub>1-*x*</sub> composites: optical property and superhydrophobicity, *Sol. Energy Mater. Sol. Cells* 180 (2018) 138–147.
- [23] I. Flores-vivian, V. Hejazi, M.I. Kozhukhova, M. Nosonovsky, K. Sobolev, Self-assembling particle-siloxane coatings for superhydrophobic concrete, *ACS Appl. Mater. Interfaces* 5 (2013) 13284–13294.
- [24] P. Liu, Y.N. Gao, F.Z. Wang, J. Yang, X.W. Yu, W.Q. Zhang, L. Yang, Superhydrophobic and self-cleaning behavior of portland cement with lotus-leaf-like microstructure, *J. Clean. Prod.* 156 (2017) 775–785.
- [25] A. Arabzadeh, H. Ceylan, S. Kim, K. Gopalakrishnan, A. Sassani, S. Sundararajan, P.C. Taylor, Superhydrophobic coatings on Portland cement concrete surfaces, *Constr. Build. Mater.* 141 (2017) 393–401.
- [26] Y. Gao, B. He, M. Xiao, Z. Fang, K. Dai, Study on properties and mechanisms of luminescent cement-based pavement materials with super-hydrophobic function, *Constr. Build. Mater.* 165 (2018) 548–559.
- [27] K. Subbiah, D.-J. Park, Y.S. Lee, V. Saraswathy, H.-S. Lee, H.-O. Jang, H.-J. Choi, Development of water-repellent cement mortar using silane enriched with nanomaterials, *Prog. Org. Coat.* 125 (2018) 48–60.
- [28] W. She, X. Wang, C. Miao, Q. Zhang, Y. Zhang, J. Yang, J. Hong, Biomimetic superhydrophobic surface of concrete: topographic and chemical modification assembly by direct spray, *Constr. Build. Mater.* 181 (2018) 347–357.
- [29] Q. Li, Z.G. Guo, Fundamentals of icing and common strategies for designing biomimetic anti-icing surfaces, *J. Mater. Chem. A* 6 (2018) 13549–13581.
- [30] W.X. Yang, Y. Yuan, G.Y. Liu, B. Zhang, R.K. Yang, The anti-icing/frosting aluminum surface with hydrangea-like micro/nano structure prepared by chemical etching, *Mater. Lett.* 226 (2018) 4–7.
- [31] M.M. Jin, Y.Z. Shen, X.Y. Luo, J. Tao, Y.H. Xie, H.F. Chen, Y. Wu, A combination structure of microblock and nanohair fabricated by chemical etching for excellent water repellency and icephobicity, *Appl. Surf. Sci.* 455 (2018) 83–890.
- [32] L. Wang, C. Teng, J. Liu, M.X. Wang, G.C. Liu, J.Y. Kim, Q.W. Mei, J.K. Lee, J.X. Wang, Robust anti-icing performance of silicon wafer with hollow micro-/nano-structured ZnO, *J. Ind. Eng. Chem.* 62 (2018) 46–51.
- [33] K. Xu, J.L. Hu, X.L. Jiang, W. Meng, B.H. Lan, L.C. Shu, Anti-icing performance of hydrophobic silicone-acrylate resin coatings on wind blades, *Coatings* 8 (2018) 151–162.
- [34] M.M. Ahmad, A. Eshaghi, Fabrication of antireflective superhydrophobic thin film based on the TMMS with self-cleaning and anti-icing properties, *Prog. Org. Coat.* 122 (2018) 199–206.
- [35] Q.Y. Hao, Y.C. Pang, Y. Zhao, J. Zhang, J. Feng, S.H. Yao, Mechanism of delayed frost growth on superhydrophobic surfaces with jumping condensates: more than interdrop freezing, *Langmuir* 30 (2014) 15416–15422.
- [36] J.L. Song, D.Y. Zhao, Z.J. Han, W. Xu, Y. Lu, X. Liu, B. Liu, C.J. Carmalt, X. Deng, I.P. Parkin, Super-robust superhydrophobic concrete, *J. Mater. Chem. A* 5 (2017) 14542–14550.
- [37] D. Kumar, X.H. Wu, Q.T. Fu, J.W.C. Ho, P.D. Kanhere, L. Li, Z. Chen, Development of durable self-cleaning coatings using organic-inorganic hybrid sol-gel method, *Appl. Surf. Sci.* 344 (2015) 205–212.
- [38] H.B. Lei, D.L. He, Y.N. Guo, Y.N. Tang, H.Q. Huang, Synthesis and characterization of UV-absorbing fluorine-silicone acrylic resin polymer, *Appl. Surf. Sci.* 442 (2018) 71–77.